

Zitterbewegung Effect in Graphene with Specially Modulated Potential

Abdellatif Kamal^a and Ahmed Jellal^{*a,b}

^a*Laboratory of Theoretical Physics, Faculty of Sciences, Chouaib Doukkali University,
PO Box 20, 24000 El Jadida, Morocco*

^b*Canadian Quantum Research Center, 204-3002 32 Ave Vernon,
BC V1T 2L7, Canada*

Abstract

The Zitterbewegung (ZB) effect is investigated in graphene with specially modulated potential near the original Dirac point (ODP) and extra Dirac points (EDPs). Our calculations show that to get the large ZB oscillations, the wave packet center must be at the angle $\theta_0 = 0$ for EDPs located at zero-energy, or $\theta_0 = \pi/2$ for both ODP and EDPs at finite energy $\varepsilon = m\pi$ (m integer). By varying the parameters (q_2, \mathbb{V}) of the periodic potential and the initial momentum (κ_0, θ_0) of Gaussian wave packet, it is found that the frequency of the ZB oscillations is in the range $[10^7 \text{ Hz}, 10^{13} \text{ Hz}]$ depending on what type of EDP is generated and the amplitude reaches hundreds of angstroms but their attenuation becomes very slow. More analysis of the frequency shows the possibilities in experimentally realizing the ZB effect in our system.

Pacs: 03.65.Pm, 72.80.Vp, 73.21.Cd, 03.65.Sq

Keywords: Graphene, specially modulated potential, extra Dirac points, Zitterbewegung effect, frequency of oscillations.

*a.jellal@ucd.ac.ma

1 Introduction

Graphene was discovered in 2004 [1] and is a single layer of carbon atoms arranged hexagonally in the honeycomb lattice. It is considered to be the miracle material of the future because of its remarkably properties. Indeed, graphene is flexible, transparent, extremely robust, can assume different electrical properties and the highest thermal conductivity of all known materials [2]. This makes it extremely interesting for potential industrial applications such as the filtration of sea water, paint, tires, internet of things, aircraft structures \dots . It is also a laboratory of experimentally testing different effects such as the quantum Hall effect and weak-localization [3]. It also allowed for the observation of some subtle effects, previously accessible only to high energy physics, like Klein tunneling and vacuum breakdown [4]. In contrary, it is difficult to observe the Zitterbewegung (ZB) effect [5] in graphene because of its high frequency and low amplitude. However, it could be possible under current experiment conditions when graphene is subject to a periodic potential [6].

The ZB effect is a rapid motion of free particles, which was originally proposed for relativistic quantum dynamics in 1930 by Schrödinger [5]. The ZB effect is a high frequency (trembling motion) of a particle in vacuum resulting from the interference between the positive and negative energy states of the relativistic Dirac particle. Recently, the ZB effect has attracted more attention because numerous theoretical work was done particularly on graphene [3, 7–11], graphene superlattices [6, 12, 13], graphene nanoribbons [14], graphene quantum dots [15]. According to [6] some conditions need to be considered in order to observe the ZB effect in graphene. Indeed, its oscillations should be sufficiently maintained over time, their frequency should be smaller than 10^{15} Hz and their amplitude must be higher than a few angstroms.

On the other hand, one of the most important features of the periodic potential is that it can decrease the group velocity of fermions near Dirac points. More precisely, we have seen that in graphene with spacially modulated potential the group velocity shows different behavior according to nature of the Dirac point [16]. It is found that its v_y -component near extra Dirac points (EDPs) at finite energy including original Dirac point (ODP) decreases remarkably but the v_x -component does not change. Such anisotropy of the group velocity is actually depending on the applied potential and therefore it is relevant to investigate its influence on the ZB effect.

We study the ZB effect of fermions in graphene with a spacially modulated potential near ODP and EDPs. Our system is a symmetrical graphene superlattice with cells of three regions [16] and two regions are separated by another one of distance q_2 . We use a method based on the implicit function to explicitly determine the dispersion relation close to a given Dirac point in terms of the group velocity components. Subsequently, we consider the Heisenberg dynamics and show that the time evolution of the position operators are functions of different physical parameters. By assuming that the initial state of Dirac fermions can be described by a two-dimensional wave packet, we show that the averages of position operators are depending on the frequency of the ZB oscillations. Later on, under various conditions of the strength of the potential, distance q_2 as well others, we numerically analyze the ZB oscillations. In particular, we show that the frequency belongs to the interval $[10^7 \text{ Hz}, 10^{13} \text{ Hz}]$ depending on the nature of EDP, the amplitude reaches hundreds of angstroms and the attenuation becomes very slow. Our results tell us that the ZB effect can be controlled by q_2 of the central region together with the potential height.

The paper is organized as follows. In section 2, we give general formulation of the problem for massless Dirac fermions in graphene with spacially modulated potential. We investigate ZB effect near different ODP and EDPs by considering the time evolution of the position operators in section 3. In section 4, we discuss the ZB oscillations under suitable conditions and make comparison with literature to show their relevance. We conclude our results in the final section.

2 Model and method

We propose another alternative way to study the ZB effect in graphene with spacially modulated potential near ODP and EDPs. Our approach is different to that used to deal with transient ZB in graphene superlattice [6]. For this, let us consider one dimensional periodic potential $V(x)$ composed of three regions growing along the x -direction with the period $d = d_1 + d_2 + d_3$. This potential is applied to graphene with the height V_i and distance d_i of each region i , as depicted in Figure 1. The Hamiltonian describing the region i of the j^{th} elementary cell can be written as

$$H = \hbar v_F(-i\sigma_x\partial_x - i\sigma_y\partial_y) + V(x)\mathbb{I}. \quad (1)$$

For convenience, we introduce dimensionless quantities $q_i = d_i/d$ ($0 \leq q_i \leq 1$), $\mathbb{V}_i = V_i/E_F$ and $\varepsilon = E/E_F$, with $E_F = \hbar v_F/d$ and $i = 1, 2, 3$. We have already studied the electronic band structures corresponding to the Hamiltonian by determining the equation governing the dispersion relation [16].

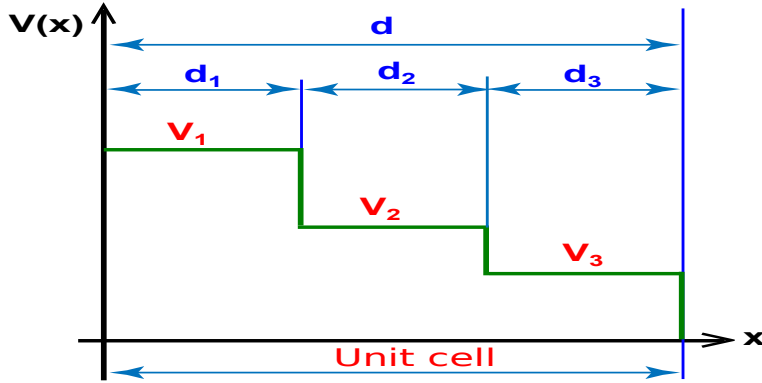


Figure 1 – (color online) Schematic of the superlattice potential $V(x)$ composed of three regions growing along the x -direction with the period $d = d_1 + d_2 + d_3$, d is the width of region i and V_i is its applied potential height.

We return back to our work [16] and review one relevant part to achieve our goals. Indeed, to explicitly determine the dispersion relation close to a given Dirac point $(k_{D_x}, k_{D_y}, \varepsilon_D)$, we introduce the implicit function $f(k_x, k_y, \varepsilon) = 0$ with

$$f(k_x, k_y, \varepsilon) = \cos(k_x d) - \cos(k_1 d_1) \cos(k_2 d_2) \cos(k_3 d_3) + G_{12} \sin(k_1 d_1) \sin(k_2 d_2) \cos(k_3 d_3) \\ + G_{13} \sin(k_1 d_1) \sin(k_3 d_3) \cos(k_2 d_2) + G_{23} \sin(k_2 d_2) \sin(k_3 d_3) \cos(k_1 d_1) \quad (2)$$

and the parameters G_{ij} are functions of the potential height and wave vectors

$$G_{ij} = \frac{(\mathbb{V}_i - \mathbb{V}_j)^2 - (k_i^2 + k_j^2)d^2}{2k_i k_j d^2}, \quad k_i = \frac{1}{d} \sqrt{(\varepsilon - \mathbb{V}_i)^2 - (k_y d)^2}. \quad (3)$$

At the Dirac point $(k_{D_x}, k_{D_y}, \varepsilon_D)$, the band structures are intersected. Then the gradient of dispersion relation must be equal zero [17], namely

$$\nabla f(k_{D_x}, k_{D_y}, \varepsilon_D) = 0. \quad (4)$$

Making the Taylor expansion of (2) around $(k_{D_x}, k_{D_y}, \varepsilon_D)$, we obtain the approximate form

$$f(k_x, k_y, \varepsilon) \approx f(k_{D_x}, k_{D_y}, \varepsilon_D) + \Delta P \nabla f(k_{D_x}, k_{D_y}, \varepsilon_D) + \frac{1}{2} \Delta P^t \mathbb{H} f(k_{D_x}, k_{D_y}, \varepsilon_D) \Delta P \quad (5)$$

where the variation ΔP and Hessian matrix \mathbb{H} are given by

$$\Delta P = \begin{pmatrix} \Delta k_x \\ \Delta k_y \\ \Delta \varepsilon \end{pmatrix} = \begin{pmatrix} k_x - k_{D_x} \\ k_y - k_{D_y} \\ \varepsilon - \varepsilon_D \end{pmatrix}, \quad \mathbb{H} f(k_{D_x}, k_{D_y}, \varepsilon_D) = \begin{pmatrix} A & 0 & 0 \\ 0 & B & 0 \\ 0 & 0 & C \end{pmatrix} \quad (6)$$

such that the parameters A , B and C are functions of the set (q_i, \mathbb{V}_i, d_i) for a given Dirac point. Now injecting (4) and (6) into (5) and using (2) to end up with

$$A\Delta k_x^2 + B\Delta k_y^2 = -C\Delta\varepsilon^2 \quad (7)$$

giving rise to the dispersion relation near the Dirac point $(k_{D_x}, k_{D_y}, \varepsilon_D)$

$$\varepsilon = \pm \sqrt{-\frac{A}{C}(k_x - k_{D_x})^2 - \frac{B}{C}(k_y - k_{D_y})^2} + \varepsilon_D \quad (8)$$

where $\text{sign}(A) = \text{sign}(B) = -\text{sign}(C)$ and the energy ε_D will be determined in the next. It is clearly see that (8) is depending on the group velocity associated to each Dirac point, such that its the two normalized components are

$$u_x = \frac{v_x}{v_F} = \frac{1}{d} \frac{\partial \varepsilon}{\partial k_x}, \quad u_y = \frac{v_y}{v_F} = \frac{1}{d} \frac{\partial \varepsilon}{\partial k_y}. \quad (9)$$

Near Dirac points, we can approximate (9) using (7) to obtain the two components

$$u_x = \frac{1}{d} \left(\frac{\Delta \varepsilon}{\Delta k_x} \right)_{\Delta k_y=0} = \frac{1}{d} \sqrt{-\frac{A}{C}}, \quad u_y = \frac{1}{d} \left(\frac{\Delta \varepsilon}{\Delta k_y} \right)_{\Delta k_x=0} = \frac{1}{d} \sqrt{-\frac{B}{C}}. \quad (10)$$

These can be implemented in (8) to get another form of the energy in terms of the wave vector

$$\varepsilon = \pm \kappa_e d + \varepsilon_D, \quad \kappa_e = \sqrt{u_x^2 (k_x - k_{D_x})^2 + u_y^2 (k_y - k_{D_y})^2}. \quad (11)$$

and therefore we can immediately realize that the corresponding Hamiltonian takes the form

$$H = \hbar v_F [u_x (k_x - k_{D_x}) \sigma_x + u_y (k_y - k_{D_y}) \sigma_y] + \varepsilon_D E_F \mathbb{I}. \quad (12)$$

This is actually different to the Hamiltonian obtained under some approximations by studying new generation of massless Dirac fermions in graphene under external periodic potential [18]. To complete the above derivation, we calculate ε_D , then in the center of the Brillouin zone we have $(k_x = 0, k_y = 0)$, which can be injected into (2) to get

$$\varepsilon_D(k_{D_x} = 0, k_{D_y} = 0) = q_1 \mathbb{V}_1 + q_2 \mathbb{V}_2 + q_3 \mathbb{V}_3 + 2n\pi, \quad n \in \mathbb{Z} \quad (13)$$

and the edge of the Brillouin zone corresponds to $(k_x = \pm \frac{\pi}{d}, k_y = 0)$, thus we obtain

$$\varepsilon_D \left(k_{D_x} = \pm \frac{\pi}{d}, k_{D_y} = 0 \right) = q_1 \mathbb{V}_1 + q_2 \mathbb{V}_2 + q_3 \mathbb{V}_3 + (2n \pm 1)\pi, \quad n \in \mathbb{Z}. \quad (14)$$

Note that, both of (13) and (14) are valid for any distance $q_i \neq 1$ and potential height \mathbb{V}_i . Recall that, the pristine graphene submitted to potential \mathbb{V}_i ($q_i = 1$) has only one Dirac point located at the energy $\varepsilon_D(k_{D_x} = k_{D_y} = 0) = \mathbb{V}_i$.

The coordinates of the Dirac points in the minibands ($k_x = \varepsilon = 0$) can be derived from the dispersion relation as

$$\frac{\mathbb{V}^2 - (k_y d)^2 \cos \left((q_2 - 1) \sqrt{\mathbb{V}^2 - (k_y d)^2} \right)}{\mathbb{V}^2 - d^2 k_y^2} \cosh(k_y q_2 d) - \frac{k_y d \sin \left((q_2 - 1) \sqrt{\mathbb{V}^2 - (k_y d)^2} \right)}{\sqrt{\mathbb{V}^2 - (k_y d)^2}} \sinh(k_y q_2 d) = 1 \quad (15)$$

which are strongly depending on the distance q_2 . Indeed, for $q_2 \neq 0$ we have only one solution $k_y = 0$ but for $q_2 = 0$ there are two

$$k_{D_y} = 0, \quad k_{D_y} = \pm \frac{1}{d} \sqrt{\mathbb{V}^2 - (2\ell\pi)^2} \quad (16)$$

and the condition $\mathbb{V}^2 > (2\ell\pi)^2$ must fulfilled with ℓ is an integer no null. Then, in minibands we have extra Dirac points ($k_x = 0, k_y = k_{Dy}, \varepsilon = 0$) in addition to the original one ($k_x = 0, k_y = 0, \varepsilon = 0$). The corresponding energies can be written in compact form as

$$\varepsilon_D = 0, \quad \varepsilon_D = q_1\mathbb{V}_1 + q_2\mathbb{V}_2 + q_3\mathbb{V}_3 + m\pi, \quad m \neq 0. \quad (17)$$

In the next, we will focus only on the case of symmetrical graphene with spacially modulated potential and under the conditions $\left(\frac{1-q_2}{2}, q_2, \frac{1-q_2}{2}\right)$, ($\mathbb{V}_1 = -\mathbb{V}_3 = \mathbb{V}$, $\mathbb{V}_2 = 0$). In this situation, (17) reduces to the following

$$\varepsilon_D = m\pi, \quad m \in \mathbb{Z}. \quad (18)$$

Now there are two cases to distinguish according to the values taken by the quantum number m and the potential height \mathbb{V} . First, if $m = 0$ and $\mathbb{V} \neq 0$, then for $q_2 = 0$ we have the velocities

$$u_x = \left(\frac{2\ell\pi}{\mathbb{V}}\right)^2, \quad u_y = 1 - \left(\frac{2\ell\pi}{\mathbb{V}}\right)^2 \quad (19)$$

and for $q_2 \neq 0$ we get

$$u_x = 1, \quad u_y(q_2, \mathbb{V}) = \frac{1}{\mathbb{V}} \sqrt{2 + q_2^2\mathbb{V}^2 - 2 \cos((q_2 - 1)\mathbb{V}) - 2q_2\mathbb{V} \sin((q_2 - 1)\mathbb{V})}. \quad (20)$$

Second, if $m \neq 0$ and $\mathbb{V} \neq |m\pi|$, then for all q_2 we find

$$\begin{aligned} u_x &= 1 \\ u_y^\pm &= \frac{\mathbb{V}}{\sqrt{2m\pi|(m\pi)^2 - \mathbb{V}^2|}} \left[3(m\pi)^2 + \mathbb{V}^2 + ((m\pi)^2 - \mathbb{V}^2) \cos(2m\pi q_2) \right. \\ &\quad \left. \pm 2m\pi \left((m\pi + \mathbb{V}) \cos(m\pi q_2 + (1 - q_2)\mathbb{V}) + (m\pi - \mathbb{V}) \cos(m\pi q_2 - (1 - q_2)\mathbb{V}) \right) \right]^{1/2} \end{aligned} \quad (21)$$

where \pm refer to odd and even integers. To allow for a better understanding, we present the obtained results in Table 1:

		Extra Dirac points ($k_{Dx}, k_{Dy}, \varepsilon_D$)			Velocity components (u_x, u_y)	
		k_{Dx}	k_{Dy}	ε_D	u_x	u_y
$m = 0$	$q_2 = 0$	0	$\pm \frac{\sqrt{\mathbb{V}^2 - (2\ell\pi)^2}}{d}, \ell \neq 0$	0	$\left(\frac{2\ell\pi}{\mathbb{V}}\right)^2$	$1 - \left(\frac{2\ell\pi}{\mathbb{V}}\right)^2$
		0	0	0	1	$u_y(0, \mathbb{V})$
	$q_2 \neq 0$	0	0	0	1	$u_y(q_2, \mathbb{V})$
$m \neq 0$	$m = 2n, n \neq 0$	0	0	$m\pi$	1	u_y^-
	$m = 2n \pm 1$	$\pm \frac{\pi}{d}$	0	$m\pi$		u_y^+

Table 1 – Coordinates of the extra Dirac points ($k_{Dx}, k_{Dy}, \varepsilon_D$) and the corresponding velocity components (u_x, u_y) for Dirac fermions in graphene with spacially modulated potential.

3 Zitterbewegung effect

We will show that in the first Brillouin zone, graphene with spacially modulated potential could influence the ZB effect under the change of the group velocities. For this, we study the dynamic of fermions described by the Hamiltonian (12) near EDPs together with ODP. Indeed, we use the Heisenberg formalism to introduce the time evolution of the position operators $x(t)$ and $y(t)$

$$x(t) = e^{-iHt/\hbar}x(0)e^{iHt/\hbar}, \quad y(t) = e^{-iHt/\hbar}y(0)e^{iHt/\hbar} \quad (22)$$

satisfying the Heisenberg equations of motion

$$\frac{dx}{dt} = u_x v_F \sigma_x, \quad \frac{dy}{dt} = u_y v_F \sigma_y. \quad (23)$$

To explicitly determine $x(t)$ and $y(t)$, we consider the dynamics of Pauli operators (σ_x, σ_y) and show the relations

$$-i\hbar \frac{d\sigma_x}{dt} = 2H\eta_x, \quad -i\hbar \frac{d\sigma_y}{dt} = 2H\eta_y \quad (24)$$

such that the operators η_x and η_y are given by

$$\eta_x = \sigma_x - \hbar u_x v_F \kappa_x H^{-1} - \varepsilon_D E_F H^{-1} \sigma_x, \quad \eta_y = \sigma_y - \hbar u_y v_F \kappa_y H^{-1} - \varepsilon_D E_F H^{-1} \sigma_y \quad (25)$$

where the wave vector $\boldsymbol{\kappa} = \mathbf{k} - \mathbf{k}_D$ has two components ($\kappa_x = k_x - k_{D_x}$, $\kappa_y = k_y - k_{D_y}$). One can show that the dynamics equations of η_x and η_y take the forms

$$-i\hbar \frac{d\eta_x}{dt} = 2H\eta_x, \quad -i\hbar \frac{d\eta_y}{dt} = 2H\eta_y \quad (26)$$

which can be solved to end up with

$$\eta_x(t) = e^{2i(H - \varepsilon_D E_F \mathbb{I})t/\hbar} \eta_{0x}, \quad \eta_y(t) = e^{2i(H - \varepsilon_D E_F \mathbb{I})t/\hbar} \eta_{0y}. \quad (27)$$

Using this together with (25) to write the dynamics (23) as

$$\frac{dx}{dt} = \hbar v_F^2 u_x^2 \kappa_x (H - \varepsilon_D E_F \mathbb{I})^{-1} + u_x v_F H (H - \varepsilon_D E_F \mathbb{I})^{-1} e^{2i(H - \varepsilon_D E_F \mathbb{I})t/\hbar} \eta_{0x} \quad (28)$$

$$\frac{dy}{dt} = \hbar v_F^2 u_y^2 \kappa_y (H - \varepsilon_D E_F \mathbb{I})^{-1} + u_y v_F H (H - \varepsilon_D E_F \mathbb{I})^{-1} e^{2i(H - \varepsilon_D E_F \mathbb{I})t/\hbar} \eta_{0y} \quad (29)$$

and their solutions can be worked out to find

$$x(t) = x_0 \mathbb{I} + u_x v_F t \sigma_x + \frac{u_x u_y \kappa_y}{2\kappa_e^2} [1 - \cos(2v_F \kappa_e t)] \sigma_z \quad (30)$$

$$+ \frac{u_x u_y \kappa_y}{2\kappa_e^3} [2v_F \kappa_e t - \sin(2v_F \kappa_e t)] (u_x \kappa_x \sigma_y - u_y \kappa_y \sigma_x)$$

$$y(t) = y_0 \mathbb{I} - u_x v_F t \sigma_y + \frac{u_x u_y \kappa_x}{2\kappa_e^2} [1 - \cos(2v_F \kappa_e t)] \sigma_z \quad (31)$$

$$+ \frac{u_x u_y \kappa_x}{2\kappa_e^3} [2v_F \kappa_e t - \sin(2v_F \kappa_e t)] (u_x \kappa_x \sigma_y - u_y \kappa_y \sigma_x)$$

where x_0 and y_0 are the constant operators of integration. It is clearly seen that the two first matrix elements are given by

$$x_{11}(t) = x_0 + \frac{u_x u_y \kappa_y}{2\kappa_e^2} [1 - \cos(2v_F \kappa_e t)] \quad (32)$$

$$y_{11}(t) = y_0 - \frac{u_x u_y \kappa_x}{2\kappa_e^2} [1 - \cos(2v_F \kappa_e t)] \quad (33)$$

Now we proceed by evaluating the averages of time-dependent position operators within a Gaussian wave packet by assuming that the initial state of Dirac fermions is described by the spinor [19]

$$\psi(\mathbf{r}, 0) = \frac{1}{2\pi} \frac{\sigma}{\sqrt{\pi}} \int d^2\boldsymbol{\kappa} e^{-\frac{1}{2}\sigma^2(\boldsymbol{\kappa}-\boldsymbol{\kappa}_0)^2} e^{i\boldsymbol{\kappa}\cdot\mathbf{r}} \begin{pmatrix} 1 \\ 0 \end{pmatrix} \quad (34)$$

where the unit vector is a convenient choice, σ and $\boldsymbol{\kappa}_0 = (\kappa_{0x}, \kappa_{0y})$ are the width and center of the wave packet, respectively. Then, the averages of the two matrix elements with respect to the spinor (34) are found to be of the forms

$$\bar{x}_{11}(t) = \frac{\sigma^2}{\pi} \int d^2\boldsymbol{\kappa} \frac{u_x u_y \kappa_y}{2\kappa_e^2} [1 - \cos(2v_F \kappa_e t)] e^{-\sigma^2(\boldsymbol{\kappa}-\boldsymbol{\kappa}_0)^2} \quad (35)$$

$$\bar{y}_{11}(t) = -\frac{\sigma^2}{\pi} \int d^2\boldsymbol{\kappa} \frac{u_x u_y \kappa_x}{2\kappa_e^2} [1 - \cos(2v_F \kappa_e t)] e^{-\sigma^2(\boldsymbol{\kappa}-\boldsymbol{\kappa}_0)^2}. \quad (36)$$

It is clearly seen that both of expressions are involving the ZB frequency $\omega(\boldsymbol{\kappa}) = 2v_F \kappa_e$ and explicitly we have

$$\omega(\boldsymbol{\kappa}) = 2\kappa v_F \sqrt{u_x^2 \cos^2 \theta_0 + u_y^2 \sin^2 \theta_0} \quad (37)$$

where the angle θ is given in terms of the wave vector

$$e^{i\theta_0} = \frac{\kappa_x + i\kappa_y}{\kappa} = \frac{u_x \kappa_x + i u_y \kappa_y}{\kappa_e} \quad (38)$$

such that $\kappa_e = (u_x \kappa_x, u_y \kappa_y)$. Note that, (37) can be determined by the difference between the upper and lower energy branches for a given wave vector $\boldsymbol{\kappa}$. It is convenient for the numerical uses to consider the average of the position operator $\bar{r}(t)$

$$\bar{r}(t) = \bar{x}_{11}(t) + i \bar{y}_{11}(t). \quad (39)$$

According to expressions (19-21) taken by the velocities u_x and u_y , we will see that (37) will provide a convenient way for adjusting the ZB oscillations by tuning on the potential height \mathbb{V} and distance q_2 of the central region.

4 Numerical results

To analyze the influence of spacially modulated potential on the ZB effect, we numerically analyze the averages of position operators \bar{x}_{11} (35), \bar{y}_{11} (36) and $|\bar{r}|$ (39) near original Dirac point (ODP) and extra Dirac points (EDPs) under suitable conditions of the set of parameters ($q_2, \mathbb{V}, d, m, \sigma, \kappa_0, \theta_0$) characterizing the applied potential and Gaussian wave packet. To carry out our computations, we take an appropriate width σ that allows investigating the influence of each extra Dirac point on the ZB effect. To avoid the ZB effect being influenced by all Dirac points and make σ not too large in momentum space, we choose one cell distance such that $d = 200 a$ as function of the interatomic distance $a = 0.142$ nm.

Figure 2 presents the ZB oscillations of the averages of position operators \bar{x}_{11} , \bar{y}_{11} and $|\bar{r}|$ versus the angle θ_0 for time $t = 50$ fs near ODP, i.e. $k_{Dx} = k_{Dy} = \varepsilon_D = 0$. In Figure 2(a), we observe that the x -direction ZB oscillation is predominate compared to the y -direction one with an amplitude very large in the vicinity of $\theta_0 = \pi/2$ [π]. In addition, there are two symmetries with respect to $\theta_0 = \pi$ such that $|\bar{r}|$ is showing symmetrical behavior while \bar{x}_{11} and \bar{y}_{11} are presenting asymmetrical ones. To shed light on the averages behaviors for small positions, we zoom one part in Figure 2(b) to show that \bar{y}_{11} presents also some pics.

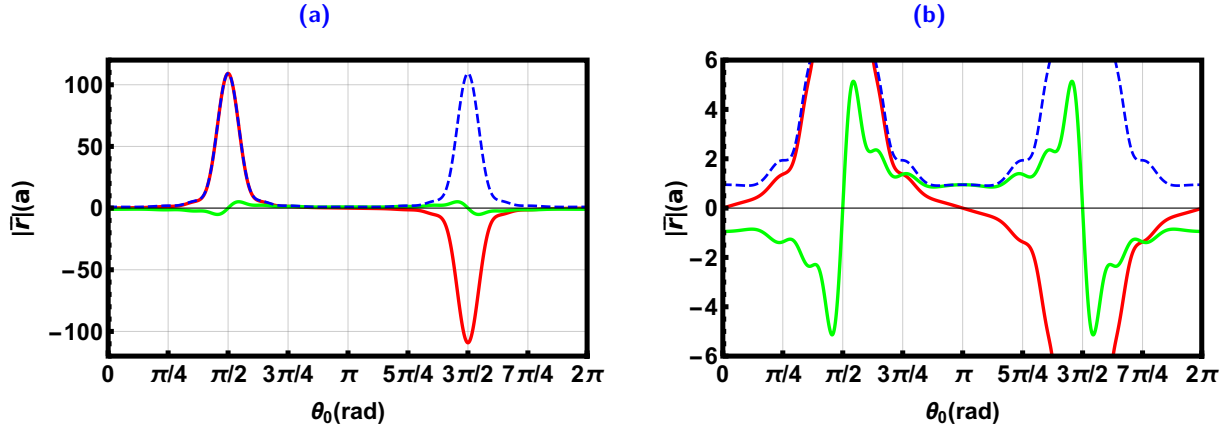


Figure 2 – (color online) (a): The averages of position operators \bar{x}_{11} (red), \bar{y}_{11} (green) and $|\bar{r}|$ (blue) versus the angle θ_0 near ODP for $t = 50$ fs, $\mathbb{V} = 7\pi$, $q_2 = 0$, $\kappa_0 = 0.05 a^{-1}$, $\sigma = 150 a$. (b): The behaviors of three averages for small values of the positions $[-6a, 6a]$.

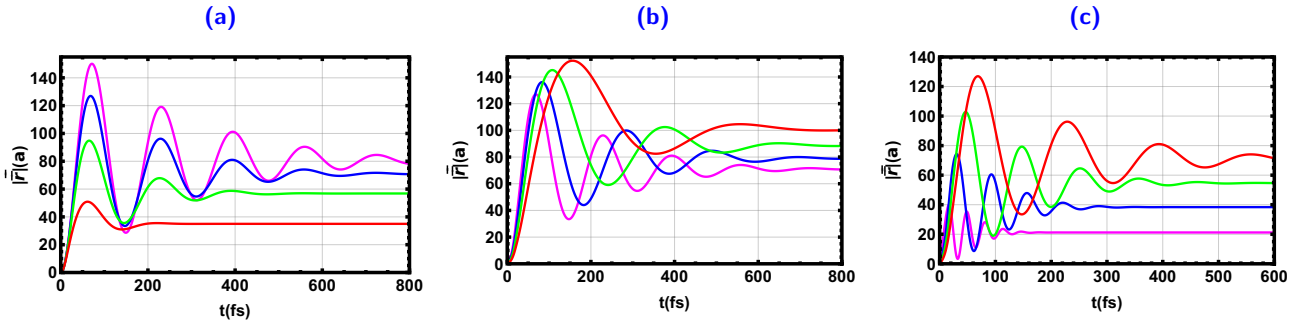


Figure 3 – (color online) The average of position operator $|\bar{r}|$ versus the time near ODP with $\mathbb{V} = 7\pi$, $\theta_0 = \pi/2$. (a): $q_2 = 0$, $\kappa_0 = 0.05 a^{-1}$ for different values of the packet width $\sigma = 50 a^{-1}$ (red), $100 a^{-1}$ (green), $150 a^{-1}$ (blue), $200 a^{-1}$ (magenta). (b): $q_2 = 0$, $\sigma = 150 a^{-1}$ for different values of the packet center $\kappa_0 = 0.02 a^{-1}$ (red), $0.03 a^{-1}$ (green), $0.04 a^{-1}$ (blue), $0.05 a^{-1}$ (magenta). (c): $\sigma = 150 a^{-1}$, $\kappa_0 = 0.05 a^{-1}$ for different values of the distance $q_2 = 0$ (red), $1/8$ (green), $1/4$ (blue), $1/2$ (magenta).

Figure 3 shows the ZB oscillations of the average of position operator $|\bar{r}|$ as function of time near ODP for $\mathbb{V} = 7\pi$, $\theta_0 = \pi/2$ and different values of the parameters (σ, κ_0, q_2). Indeed, in Figure 3(a) with $\kappa_0 = 0.05 a^{-1}$ and $q_2 = 0$, we clearly see that by increasing the packet width σ , the amplitude of the ZB oscillations becomes large and the attenuation becomes slow. In fact, for small σ there are no oscillations while for very large σ the ZB oscillations are nearly undamped. We notice that the period of the ZB oscillations is weakly depending on σ , but the corresponding amplitudes are strongly depending on σ , which is consistent with the previous analysis in literature [6, 20]. In Figure 3(b) with $\sigma = 150 a^{-1}$ and $q_2 = 0$, it is found that the amplitude and period of the ZB oscillations decrease, but the attenuation remains constant. This can be explained by the fact that the initial normalized frequency $\omega = \omega(\kappa_0)$ of the ZB oscillations takes the form

$$\frac{\omega}{\omega_0} = \frac{\sqrt{2 - 2 \cos \mathbb{V}}}{\mathbb{V}}, \quad \omega_0 = 2\kappa_0 v_F \quad (40)$$

which exactly coincides with the normalized group velocity u_y along the y -direction that can be obtained from (20) by requiring $q_2 = 0$. This clearly shows that the velocity u_y affects the ZB oscillations near ODP. To observe the ZB effect in the vicinity of ODP, we should not apply a potential of the form $\mathbb{V} = 2n\pi$ (n is integer) because according to (40) the frequency ω will be null. Contrariwise, for such potential $\mathbb{V} = 2n\pi$ and from (37) we show that the frequency is of order 10^{13} Hz. In Figure 3(c) with

$\sigma = 150 \text{ a}^{-1}$ and $\kappa_0 = 0.05 \text{ a}^{-1}$, we observe that as the distance increases from $q_2 = 0$ to $q_2 = 1/2$, the period, amplitude and attenuation of the ZB oscillations outstandingly reduce.

Now we examine the case where the angle is fixed as $\theta_0 = \pi/2$. Then, the initial normalized frequency of the ZB oscillations (37) reduces to

$$\frac{\omega}{\omega_0} = \frac{1}{\mathbb{V}} \sqrt{2 + q_2^2 \mathbb{V}^2 - 2 \cos((q_2 - 1) \mathbb{V}) - 2q_2 \mathbb{V} \sin((q_2 - 1) \mathbb{V})} \quad (41)$$

which is plotted in Figure 4 versus the distance q_2 for $\mathbb{V} = 7\pi$. For m an odd integer and $q_2 = 0$, the frequency is nonzero and decreases as long as \mathbb{V} increases. However, for any even integer value of m , the frequency is zero for $q_2 = 0$. On the other hand, it is clearly seen that when q_2 increases ω/ω_0 also increases. In addition, the frequency ω/ω_0 oscillates around the straight line $\omega/\omega_0 = q_2$, but for a large value of the potential height \mathbb{V} , we have exactly the convergence $\omega/\omega_0 = q_2$. These results tell us that the ZB oscillations in the vicinity of ODP can be controlled by the parameters \mathbb{V} and q_2 .

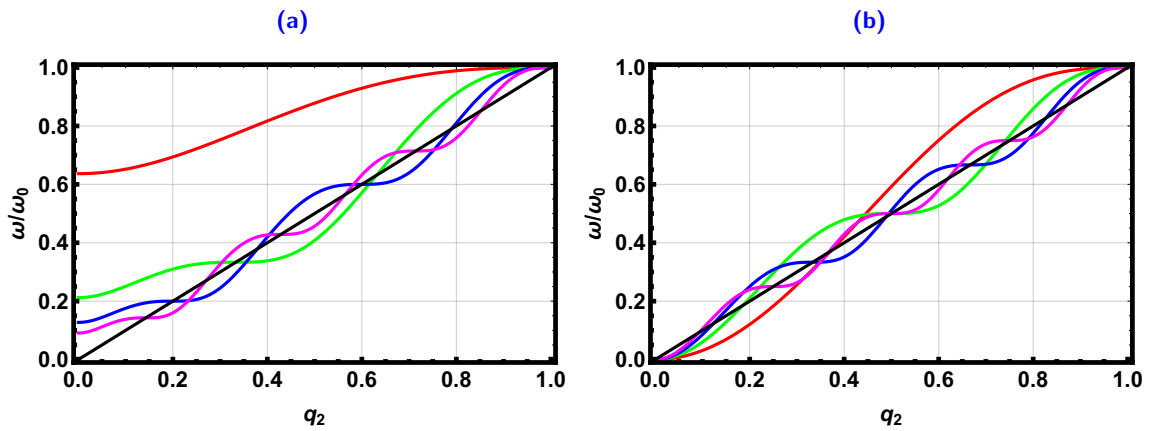


Figure 4 – (color online) The initial normalized frequency ω/ω_0 of the ZB oscillations versus the distance q_2 for $\mathbb{V} = m\pi$, with m is integer. (a): Odd values $m = 1$ (red), 3 (green), 5 (blue), 7 (magenta). (b): Even values $m = 2$ (red), 4 (green), 6 (blue), 8 (magenta). In both Figures the limiting case $\mathbb{V} \rightarrow \infty$ (black) is considered.

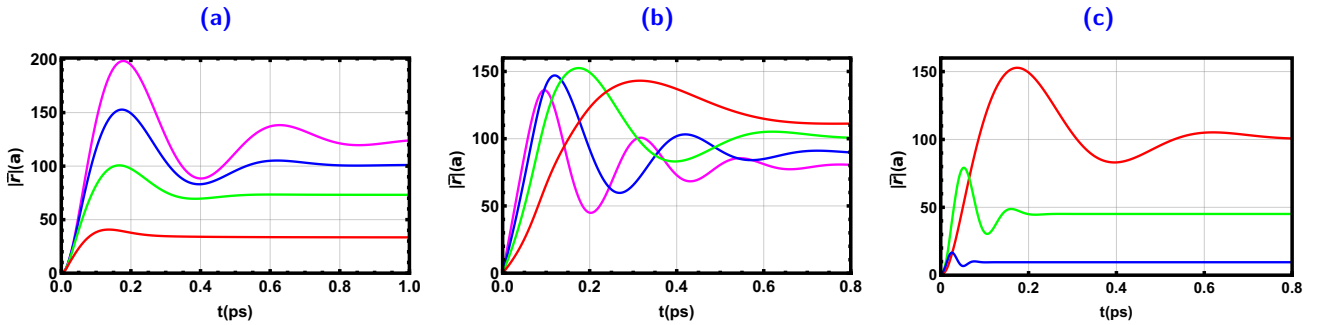


Figure 5 – (color online) The average of position operator $|\bar{r}|$ versus the time near EDPs located at zero energy for $q_2 = 0$, $\mathbb{V} = 7\pi$, $\theta_0 = 0$. (a): $\ell = 1$, $\kappa_0 = 0.02 \text{ a}^{-1}$ for different values of the wave packet width $\sigma = 50 \text{ a}^{-1}$ (red), 100 a^{-1} (green), 150 a^{-1} (blue), 200 a^{-1} (magenta). (b): $\ell = 1$, $\sigma = 150 \text{ a}^{-1}$ for different values of $\kappa_0 = 0.02 \text{ a}^{-1}$ (red), 0.03 a^{-1} (green), 0.04 a^{-1} (blue), 0.05 a^{-1} (magenta). (c): $\sigma = 150 \text{ a}^{-1}$, $\kappa_0 = 0.02 \text{ a}^{-1}$ for different values of $\ell = \pm 1$ (red), ± 2 (green), ± 3 (blue).

In addition of ODP, we have EDPs located at $(k_{Dx} = 0, k_{Dy} = \pm\sqrt{\mathbb{V}^2 - (2\ell\pi)^2}/d, \varepsilon_D = 0)$ with $\ell \neq 0$ and $\mathbb{V} \geq 2\ell\pi$. To study ZB oscillations near these EDPs, we choose $\mathbb{V} = 7\pi$, in order to have three EDPs at $\varepsilon = 0$. Figure 5 shows the ZB oscillations of the average of position operator $|\bar{r}|$ as function of the time near the first EDP at zero energy for $q_2 = 0$, $\mathbb{V} = 7\pi$, $\theta_0 = 0$ and different values of the

parameters (σ, κ_0, ℓ) . In Figure 5(a) with $\kappa_0 = 0.02 a^{-1}$ and $\ell = 1$, it is found that for small σ there are no oscillations. Increasing σ , the amplitude of the ZB oscillations become larger compared to that of ODP and the attenuation becomes slow. In Figure 5(b) with $\sigma = 150 a^{-1}$ and $\ell = 1$, we consider different values of the initial momentum κ_0 and show that by decreasing κ_0 the amplitudes of the ZB oscillations decrease, the frequency increases and the attenuation remains constant. In Figure 5(c) with $\sigma = 150 a^{-1}$ and $\kappa_0 = 0.02 a^{-1}$, for different values of ℓ we observe that by increasing ℓ the amplitudes, period and the attenuation decrease, which is quiet normal because we have the relation

$$\frac{\omega}{\omega_0} = \frac{2\ell\pi}{\mathbb{V}}. \quad (42)$$

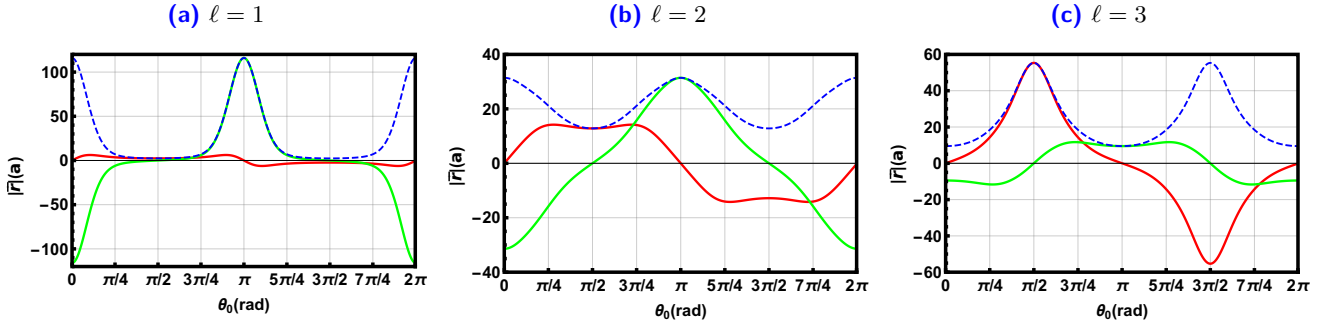


Figure 6 – (color online) The averages of position operators \bar{x}_{11} (red), \bar{y}_{11} (green) and $|\bar{r}|$ (blue) versus the angle θ_0 near EDPs located at zero energy $\varepsilon_D = 0$ for $t = 0.1$ ps, $q_2 = 0$, $\mathbb{V} = 7\pi$, $\sigma = 150 a^{-1}$, $\kappa_0 = 0.02 a^{-1}$ and three values of the quantum number $\ell = 1, 2, 3$.

Figure 6 presents the averages of position operators \bar{x}_{11} (red), \bar{y}_{11} (green) and $|\bar{r}|$ (blue) as function of the angle θ_0 for time $t = 0.1$ ps. It is clearly seen that for $\ell = 1$, it shows that the y -direction ZB oscillation is predominate compared to the x -direction one. The amplitude of the y -direction ZB oscillation is very large in the vicinity of $\theta_0 = 0$ [π]. Now for $\ell = 2$, the amplitude of x -direction ZB oscillation increases but that of the y -direction decreases. Finally for $\ell = 3$, the amplitude of the x -direction ZB oscillation is still increasing to reach large value in the vicinity of $\theta_0 = \pi/2$ [π]. In all cases, we observe that the behavior of $|\bar{r}|$ shows different periodicity with respect to $\theta_0 = \pi/2$.

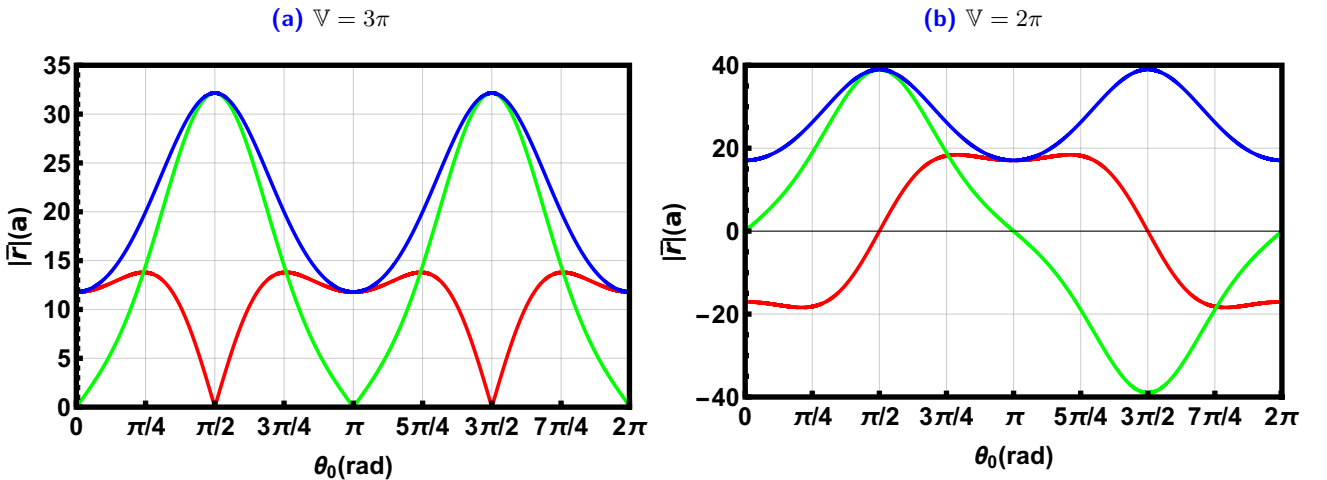


Figure 7 – (color online) The averages of position operators \bar{x}_{11} (red), \bar{y}_{11} (green) and $|\bar{r}|$ (blue) versus the angle θ_0 for $t = 14$ fs, $q_2 = 1/3$, $\kappa_0 = 0.03 a^{-1}$. (a): near EDPs located at finite energy $\varepsilon_D = 2\pi$ with $k_{D_x} = k_{D_y} = 0$. (b): near EDPs located at finite energy $\varepsilon_D = \pi$ with $k_{D_x} = \pm\pi/d$, $k_{D_y} = 0$.

In Figure 7, we present the averages of position operators \bar{x}_{11} (red), \bar{y}_{11} (green) and $|\bar{r}|$ (blue) versus the angle θ_0 near EDPs located at finite energy $\varepsilon_D = 2\pi$ ($\varepsilon_D = \pi$) for $t = 14$ fs, $\sigma =$, $q = 1/3$, $\kappa_0 = 0.03 a^{-1}$. In the present situation, we consider two interesting cases, for $\theta_0 \neq \pi/2$ [π] we observe that both x - and y -direction ZB oscillations exist but show different behaviors. For $\theta_0 = \pi/2$ [π], it appears that the amplitude of the x -direction ZB oscillations is null while that of y -direction becomes maximal.

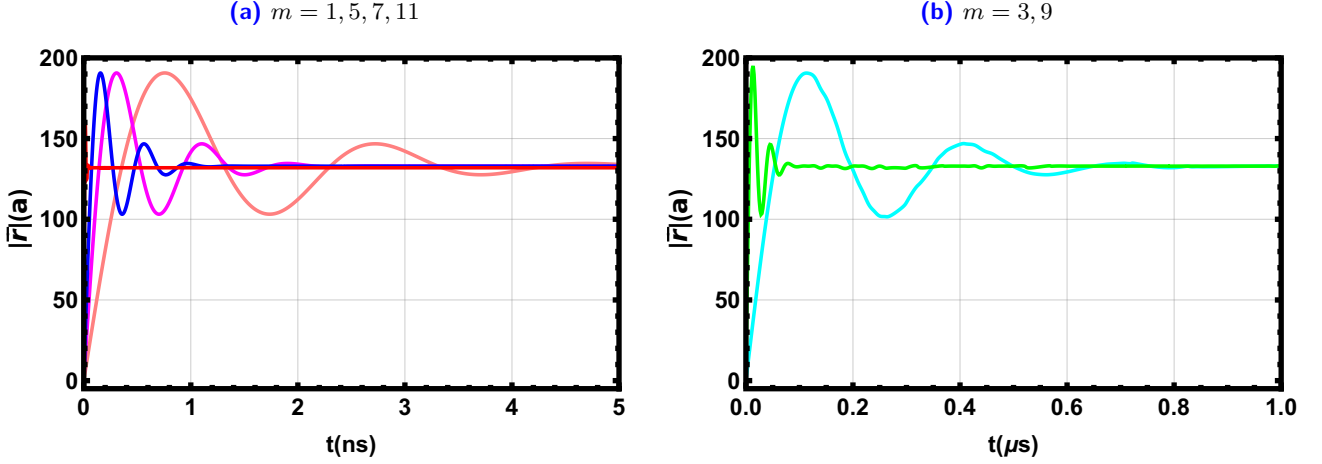


Figure 8 – (color online) The average of position operator $|\bar{r}|$ versus the time near EDPs located at finite energy energy $\varepsilon_D = \pi m$ with $m = 2n \pm 1$ for $q_2 = 1/3$, $\mathbb{V} = 0.01\pi$, $\theta_0 = \pi/2$, $\kappa_0 = 0.03 a^{-1}$. (a): $m = 1$ (red), 5 (blue), 7 (magenta), 11 (pink). (b): $m = 3$ (green), 9 (cyan).

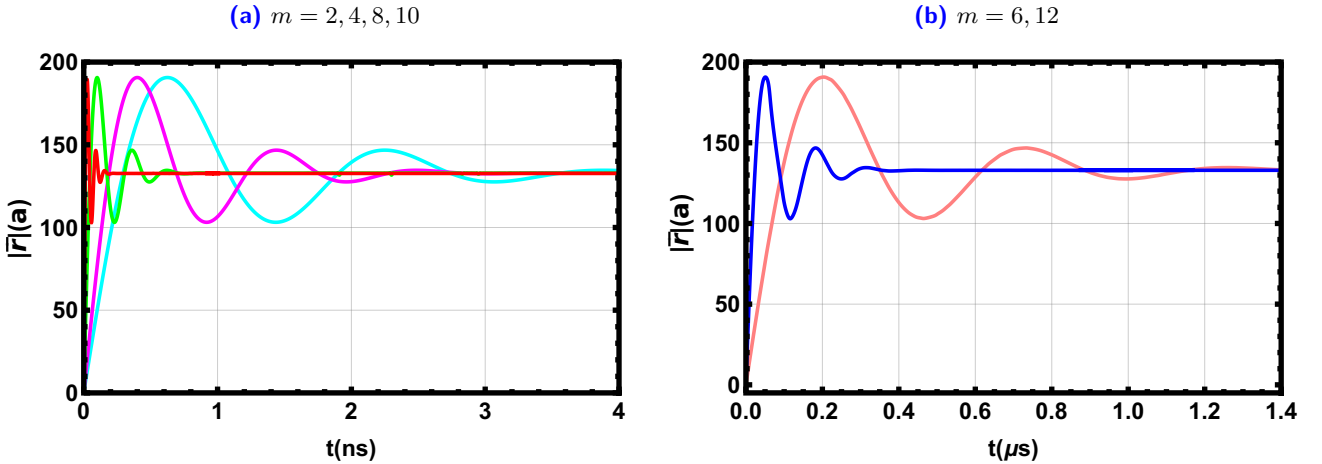


Figure 9 – (color online) The ZB oscillation versus time near EDPs located at finite energy energy $\varepsilon_D = \pi m$ with $m = 2n \neq 0$ for $q_2 = 1/3$, $\mathbb{V} = 0.01\pi$, $\theta_0 = \pi/2$, $\kappa_0 = 0.03 a^{-1}$. (a): $m = 2$ (red), 4 (green), 8 (magenta), 10 (cyan). (b): $m = 6$ (blue), 12 (pink).

To get maximal ZB oscillations in our system, we analyze the situations where the angle takes the value $\theta_0 = \pi/2$. Indeed, Figure 8 (9) illustrates the ZB oscillations of the average of position operator $|\bar{r}|$ versus the time near EDPs located at finite energy $\varepsilon_D = \pi m$ with $m = 2n \pm 1$ ($m = 2n \neq 0$) for some values of m . As long as m increase, the frequency of ZB oscillations decreases except for $m = 3$, 9 ($m = 6$, 12). The period of ZB oscillations can reach a few nanoseconds, while the amplitude of oscillations remains almost constant and the frequency is much lower than that found in [6, 13]. However, the frequency decreases remarkably in the case of $m = 3$, 9 ($m = 6$, 12). To understand why there is such decrease in the frequency, it suffices to write the initial normalized frequency, using Table 1, in terms of

the normalized velocities

$$\frac{\omega}{\omega_0} = \begin{cases} u_y^+ & \text{if } m = 2n \pm 1 \\ u_y^- & \text{if } m = 2n \neq 0. \end{cases} \quad (43)$$

Figure 10 shows the initial normalized frequency ω/ω_0 versus the quantum number m for $q_2 = 1/3$ and $\mathbb{V} = 0.01\pi$. It is clearly seen that ω/ω_0 has the minima located at points $m = 6k + 1$ ($m = 3(2k + 1)$) with k is integer. For $m = 6k$, the frequency reaches 10^8 Hz and it is of order 10^9 Hz, 10^8 Hz, 10^7 Hz for $m = 3, 9, 15$, respectively. While, the amplitude of the ZB oscillations is of order $200 a$. This result suggest that graphene with spacially modulated may provide a good system to experimentally study the ZB effect near EDPs.

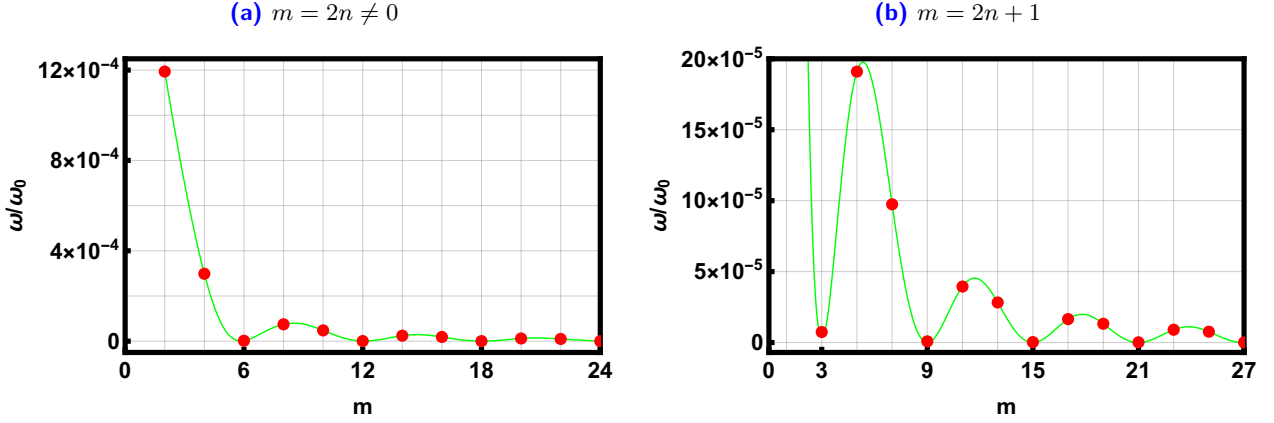


Figure 10 – (color online) Initial normalized frequency ω/ω_0 versus the quantum number m for $\mathbb{V} = 0.01\pi$ and $q_2 = 1/3$.

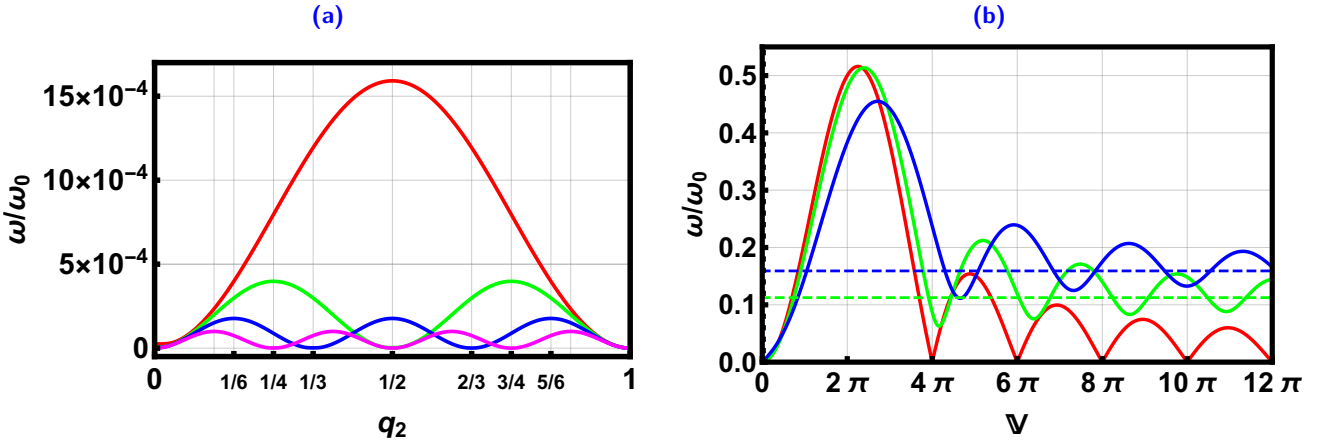


Figure 11 – (color online) The initial normalized frequency ω/ω_0 such that (a): versus the distance q_2 with $\mathbb{V} = 0.01\pi$ for some values of $m = 2$ (red), 4 (green), 6 (blue), 8 (magenta), (b): versus the potential height \mathbb{V} with $m = 2$ for three values of the distance $q_2 = 0$ (red), $1/8$ (green), $1/4$ (blue).

Figures 11(a) and 12(a) elucidate the initial normalized frequency ω/ω_0 versus the distance q_2 with $\mathbb{V} = 0.01$ for some values of m . As long as m increases, ω/ω_0 decreases and the corresponding number of peaks increases. We notice that, for $m = 2n \neq 0$, ω/ω_0 has n maxima and $n - 1$ minima. In Figure 11(b) and 12(b), we present the initial normalized frequency ω/ω_0 versus the potential height \mathbb{V} with some values of q_2 for $m = 2$. According to Figure 11(b) (12(b)), we summarize the following interesting results. Indeed, when q_2 increases, the amplitude of oscillations of ω/ω_0 decreases and its periodicity

increases as long as \mathbb{V} increases. Up to a large value of \mathbb{V} , we obtain

$$\lim_{\mathbb{V} \rightarrow +\infty} \frac{\omega}{\omega_0} = \frac{|\sin(q_2 m \pi)|}{m \pi}. \quad (44)$$

For $q_2 = 0$, we observe there are different oscillations appearing between each 2π and their amplitudes decrease when \mathbb{V} increases except for the interval $[2\pi, 4\pi]$ ($[\pi, 3\pi]$). In addition, the values for $\omega/\omega_0 = 0$ coincide with those where EDPs appear, namely $\mathbb{V} = (k+1)\pi$ ($\mathbb{V} = (2k+1)\pi$) except for $\mathbb{V} = 2\pi$ ($\mathbb{V} = \pi$) because for a given m the potential height should be $\mathbb{V} \neq m\pi$. For a given m , the peak of ω/ω_0 is located at a potential height greater than $m\pi$.

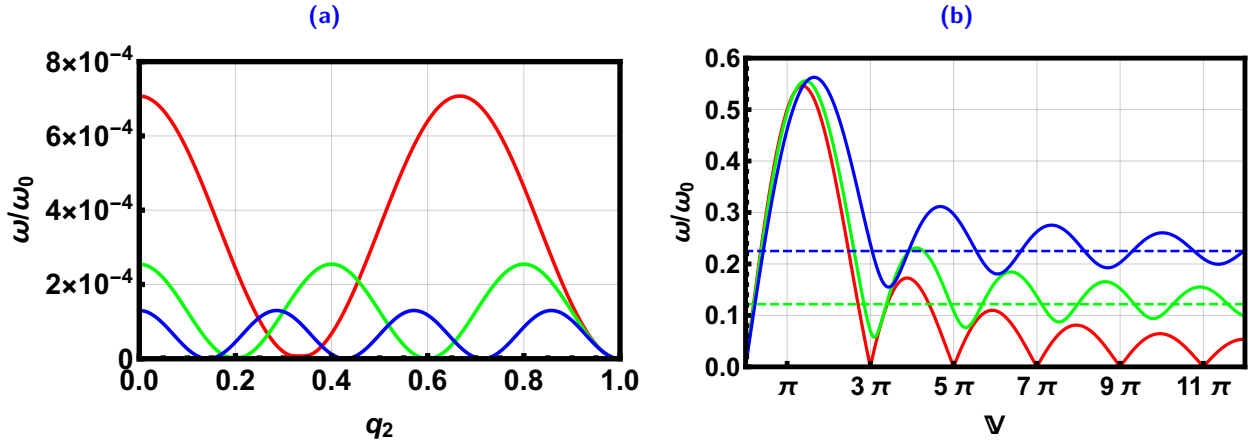


Figure 12 – (color online) The initial normalized frequency ω/ω_0 such that (a): versus the distance q_2 with $\mathbb{V} = 0.01\pi$ for some values of $m = 1$ (red), 3 (green), 5 (blue), 7 (magenta). (b): versus the potential height \mathbb{V} with $m = 1$ for three values of the distance $q_2 = 0$ (red), $1/8$ (green), $1/4$ (blue).

Conclusion

We have studied the Zitterbewegung (ZB) effect of massless Dirac fermions in graphene with spacially modulated potential near original Dirac point (ODP) extra Dirac points (EDPs). In the first Brillouin zone, we have seen that our system could influence the ZB effect by changing the group velocity of fermions. Such velocity is maximal along the superlattice direction and minimal along the perpendicular one. Subsequently, using a Gaussian wave packet with finite momentum κ_0 , we have shown that the frequency of the ZB oscillations can be influenced by the applied potential parameters such as the distance q_2 , potential height \mathbb{V} , momentum κ_0 , angle θ_0 together with EDPs.

The numerical calculations showed that to get the large ZB oscillations, the wave packet center should be at $\theta_0 = 0$ for EDPs located at zero-energy or at $\theta_0 = \pi/2$ for ODP and EDPs located at finite energy $\varepsilon = m\pi$, with m is integer. We have seen that the amplitude of the ZB oscillations can reach hundreds of angstroms and their frequency can be in the interval $[10^7 \text{ Hz}, 10^9 \text{ Hz}]$. We have shown that its attenuation can be slowly transient and can reach a few nanoseconds until microseconds, which can be clearly detected. Our results suggest that the present system may provide an appropriate candidate to experimentally realize the ZB effect near EDPs.

Acknowledgment

The generous support provided by the Saudi Center for Theoretical Physics (SCTP) is highly appreciated by all authors.

References

- [1] K. S. Novoselov, A. K. Geim, S. V. Morozov, D. Jiang, Y. Zhang, S. V. Dubonos, I. V. Grigorieva, A. A. Firsov, *Science* **306**, 666 (2004).
- [2] A. H. Castro Neto, F. Guinea, N. M. R. Peres, K. S. Novoselov, and A. K. Geim *Rev. Mod. Phys.* **81**, 109 (2009).
- [3] K. S. Novoselov, A. K. Geim, S. V. Morozov, D. Jiang, M. I. Katsnelson, I. V. Grigorieva, S. V. Dubonos, and A. A. Firsov, *Nature* **438**, 197 (2005).
- [4] M. I. Katsnelson and K. S. Novoselov, *Solid State Commun.* **143**, 3 (2007).
- [5] E. Schrödinger, *Sitzungsber. Preuss. Akad. Wiss. Phys.-Math. Kl.* **24**, 418 (1930).
- [6] Q. Wang, R. Shen, L. Sheng, B. G. Wang, and D. Y. Xing, *Phys. Rev. A* **89**, 022121 (2014).
- [7] T. M. Rusin and W. Zawadzki, *Phys. Rev. B* **76**, 195439 (2007); *ibid* **78**, 125419 (2008).
- [8] G. M. Maksimova, V. Y. Demikhovskii, and E. V. Frolova, *Phys. Rev. B* **78**, 235321 (2008).
- [9] E. Romera and F. de los Santos, *Phys. Rev. B* **80**, 165416 (2009).
- [10] A. Chaves, L. Covaci, K. Y. Rakhimov, G. A. Farias, and F. M. Peeters, *Phys. Rev. B* **82**, 205430 (2010).
- [11] J. Cserti and G. Dávid, *Phys. Rev. B* **74**, 172305 (2006).
- [12] H. Deng, F. Ye, B. A. Malomed, X. Chen, and N. C. Panoiu, *Phys. Rev. B* **91**, 201402 (2015).
- [13] J. Luan, S. Li, T. Ma, and L.-G. Wang, *J. Phys.: Condens. Matter* **30**, 395502 (2018).
- [14] S. Ghosh, U. Schwingenschlögl, and A. Manchon, *Phys. Rev. B* **91**, 045409 (2015).
- [15] T. García, N. A. Cordero, and E. Romera, *Phys. Rev. B* **89**, 075416 (2014).
- [16] A. Kamal, E. B. Choubabi, and A. Jellal, *Eur. Phys. J. B* **91**, 91 (2018).
- [17] J. R. Lima, *Phys. Lett. A* **379**, 1372 (2015).
- [18] C.-H. Park, L. Yang, Y.-W. Son, M. L. Cohen, and S. G. Louie, *Phys. Rev. Lett.* **101**, 126804 (2008).
- [19] J. Schliemann, D. Loss, and R. M. Westervelt, *Phys. Rev. Lett.* **94**, 206801 (2005); *Phys. Rev. B* **73**, 085323 (2006).
- [20] X. Zhang, *Phys. Rev. Lett.* **100**, 113903 (2008).